Classical dynamics of the time-dependent elliptical billiard

Florian Lenz,[1,*] Fotis K. Diakonos,[2] and Peter Schmelcher[1,3]
[1]*Physikalisches Institut, Universität Heidelberg, Philosophenweg 12, 69120 Heidelberg, Germany*
[2]*Department of Physics, University of Athens, GR-15771 Athens, Greece*
[3]*Theoretische Chemie, Institut für Physikalische Chemie, Universität Heidelberg, INF 229, 69120 Heidelberg, Germany*
(Received 16 February 2007; revised manuscript received 19 July 2007; published 28 December 2007)

In this work we study the nonlinear dynamics of the static and the driven ellipse. In the static case, we find numerically an asymptotical algebraic decay for the escape of an ensemble of noninteracting particles through a small hole due to the integrable structure of the phase space of the system. Furthermore, for a certain hole position, a saturation value in the decay that can be tuned arbitrarily by varying the eccentricity of the ellipse is observed and explained. When harmonic boundary oscillations are applied, this saturation value, caused by librator-type orbits, is gradually destroyed via two fundamental processes which are discussed in detail. As a result, an amplitude-dependent emission rate is obtained in the long-time behavior of the decay, suggesting that the driven elliptical billiard can be used as a controllable source of particles.

DOI: 10.1103/PhysRevE.76.066213 PACS number(s): 05.45.Ac, 05.45.Pq, 05.45.Gg

I. INTRODUCTION

Billiards belong to the most widely studied class of Hamiltonian systems. They possess many of the classical and quantum mechanical properties of complex dynamical systems [1–3]. Moreover, models of statistical mechanics can be reduced to billiards [4]. For example, one of the simplest cases of billiards, particles inside a rectangular box, is an idealization of the physical situation of nucleons confined inside a nucleus [5]. Mathematically rigorous studies of billiards go back to the early 1970s, e.g., Bunimovich proved that stadia are ergodic [6], using concepts developed by Sinai. In recent years, a renewed interest in billiards has come up, due to the possibilities of realizing them experimentally, for example by using ultracold atoms confined in a laser potential [7], microwave billiards [2,8,9], or mesoscopic quantum dots [10]. Even for the design of directional microlasers, billiards are relevant [11]. Besides this, interesting theoretical results have been obtained, including a justification for a probabilistic approach to statistical mechanics [4,12]. Very recently, it has been shown [13] that a connection exists between billiards and one of the major unsolved problems in mathematics, the Riemann hypothesis: the authors of [13] found an analytic expression for the escape rate of a circular billiard with two holes, involving a sum over the zeros of the Riemann ζ function.

A natural generalization of billiards with a static boundary is to apply a driving law to the billiard wall. For instance, Bohr's liquid drop model from nuclear physics can be regarded as a time-dependent billiard [14]. For this simple-looking model, many questions still remain open [15]. Another example is in plasma physics, where time-dependent billiards represent models for acceleration of particles in a magnetic bottle (see [16] and references therein). In conclusion, there are many branches of physics in which billiards, specifically time-dependent billiards, serve as models for more complex systems, capturing the key features and behavior of the original problem.

Ultracold atoms in a billiard formed by beams of light allow for the possibility of generating arbitrary geometries and changing them in time, as well as varying parameters such as beam width, softness of the potential, etc. in time. Of special interest is the possibility of probing the dynamics by analyzing the escape rates [7,17–20], which has up to date been performed only for static billiards. Introducing noise and decoherence and studying the role of quantum and many-body effects are further intriguing goals [7].

Regarding time-dependent billiards, there exist several investigations in the literature [16,21–28]. A crucial question for these systems is whether Fermi acceleration occurs or not. This is examined in Refs. [21–24] and very recently in Ref. [27]. In [21] it is shown that, when using smooth forcing functions, the existence of invariant spanning Kolmogorov-Arnold-Moser curves in phase space limits the energy gain of the particles, whereas nonsmooth forcing functions, especially random oscillation, lead to unbounded energy gain; see also Ref. [27] and references therein. In Ref. [22], the authors conclude with the hypothesis: "A random element in a billiard with a fixed boundary is a sufficient condition for the Fermi acceleration in the system when a boundary perturbation is introduced."

Within the existing studies of classical time-dependent billiards only little emphasis is put on systems with a finite horizon and (to our knowledge) none on the corresponding escape rates. Very few works deal with the time-dependent ellipse [16,25,26]. In Ref. [16], the average velocity as a function of time and the Poincaré surface of section of the dynamics of the ellipse for different driving laws are studied numerically. Depending on the driving laws and the initial velocity of an ensemble, the integrable structure of the phase space is more or less destroyed compared to the static case. The velocity of the particles stays bounded in all cases, i.e., no Fermi acceleration occurs. The authors point out that all conditions are satisfied in order to apply Douady's theorem [29], which predicts this boundedness of the velocity. A mathematical study of periodically driven ellipses is given in [25]. The authors show that, in principle, it is possible to destroy the diametral two-periodic orbit via boundary oscillations, and give strong evidence that the opposite—

*lenz@physi.uni-heidelberg.de

stabilizing an unstable periodic orbit with the use of driving—is not possible.

The above discussion shows that very little is known about escape rates in classical time-dependent billiards. Apart from being of fundamental interest, this type of driven dynamical system is nowadays well within the reach of experiments, as indicated above. Moreover, our investigation will demonstrate that time-dependent billiards might provide us with a tunable source of particles. As we shall see, the escape rate and the velocity distribution of the escaping particles strongly depend on the driving properties, such as the amplitude and frequency of periodic driving.

In this work, which is an extension of our recently published Letter [30], we focus on the driven elliptical billiard. Its static counterpart is integrable, due to the existence of a second constant of motion, the product of the angular momenta around the foci. Thus the phase space of the ellipse possesses a more complex structure, consisting of librators and rotators, than the prototype integrable billiard, the circle. Naturally, it would also be interesting to study driven billiards whose static counterparts have mixed or chaotic dynamics. Yet the clear partition of the phase space into librators and rotators of the ellipse considerably simplifies the analysis in the presence of the driving. This allows us to study, e.g., transition between librator and rotator orbits and to discuss associated physical phenomena in an intuitive way.

This paper is structured as follows. In Sec. II we discuss fundamental properties and escape rates in the static ellipse. The generalization to time-dependent ellipses is treated in Sec. III. The fundamental processes leading to the destruction of the librator orbits are displayed in Sec. III C, followed by an analysis of the angular momentum, Sec. IV, and the velocity, Sec. V. Finally, a summary is given in the last section.

II. STATIC ELLIPSE

A. Fundamental properties of the dynamics in the ellipse

In a two-dimensional static billiard, the orbit of a particle can be completely specified by providing the sequence of its positions s_i (measured by the arclength) or φ_i [see Eq. (1)] on the boundary $\mathcal{B}$ and the directions $p_i=\cos\alpha_i$ immediately after each collision, since the particles travel ballistically in between collisions, where α_i is the angle between the forward pointing tangent and the velocity of the particle at the ith collision point. The corresponding discrete mapping $\mathcal{M}$ is area preserving in the phase space variables s and p [1]. The boundary $\mathcal{B}$ of an ellipse is given by

$$\mathcal{B}=\{x(\varphi)=A\cos\varphi, y(\varphi)=B\sin\varphi)|0\leqslant\varphi<2\pi\} \quad (1)$$

with $A>B>0$, A and B being the long and the short half diameter, respectively. The dimensionless numerical eccentricity can be written as $\varepsilon=\sqrt{1-B^2/A^2}$.

In anticipation of the time-dependent problem, we describe the direction of a particle by its velocity $\boldsymbol{v}=(v_x,v_y)$. If we demand without loss of generality $|\boldsymbol{v}|=1$, there is a one-to-one correspondence between the velocity $\boldsymbol{v}$ and p at the collision points. At a certain time t, the position of the particle starting at $t=0$ at $\boldsymbol{x}_0=(x_0,y_0)\in\mathcal{B}$ with the velocity $(v_{x,0},v_{y,0})$ is given by

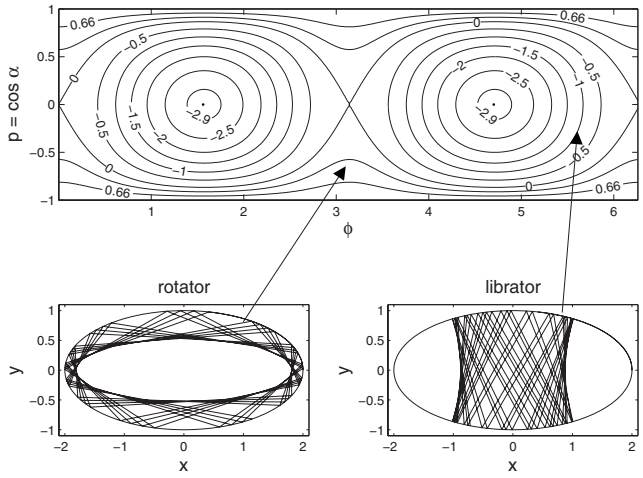

FIG. 1. PSS of the ellipse (upper part) and typical trajectories (lower part), $A=2$, $B=1$. The rotator orbit repeatedly touches a confocal ellipse, the librator orbit a confocal hyperbola.

$$x(t)=x_0+v_{x,0}t, \quad (2a)$$

$$y(t)=y_0+v_{y,0}t. \quad (2b)$$

The particle will hit the boundary at $\boldsymbol{x}_1$ at the time t_1.

$$t_1=-\frac{2B^2x_0v_{x,0}+2A^2y_0v_{y,0}}{(Av_{y,0})^2+(Bv_{x,0})^2}. \quad (3)$$

To get the new velocity $\boldsymbol{v}_1$, we parametrize $\boldsymbol{x}_1\in\mathcal{B}$ by φ_1 and calculate the inward pointing normal vector $\hat{\boldsymbol{n}}_1, |\hat{\boldsymbol{n}}_1|=1$, at φ_1. This results in

$$\boldsymbol{v}_1=\boldsymbol{v}_0-2(\hat{\boldsymbol{n}}_1\cdot\boldsymbol{v}_0)\cdot\hat{\boldsymbol{n}}_1. \quad (4)$$

Equation (4) can be easily extended to time-dependent boundaries (see Sec. III), where momentum transfer from the moving wall to the particle takes place.

The dynamics in the ellipse is completely integrable (see Fig. 1). In addition to the energy, there is another constant of motion $F(\varphi,p)$, restricting the orbits to invariant curves in phase space:

$$F(\varphi,p)=\frac{p^2[1+(1-\varepsilon^2)\cot^2\varphi]-\varepsilon^2}{1+(1-\varepsilon^2)\cot^2\varphi-\varepsilon^2}. \quad (5)$$

$F(\varphi,p)$ can be interpreted as the product of the angular momenta (PAM) about the two focus points [1]. There are two different types of orbits, rotators and librators, in the ellipse, separated by the separatrix (see Fig. 1). Librators cross the x axis between the two focus points and repeatedly touch a confocal hyperbola. In the Poincaré surface of section (PSS), they appear as deformed circles around elliptic fixed points, exploring a limited range in p as well as in φ. Rotator orbits travel around the ellipse, exploring every value of φ, but only a small range in p (except if they are very close to the separatrix), repeatedly touching a confocal ellipse.

In terms of $F(p,\varphi)$, we can distinguish three different cases.

(1) $F(\varphi,p)>0$ corresponds to the rotator orbits with an elliptical caustic.

(2) $F(\varphi,p)<0$ are the librators with hyperbolic caustic. This includes the two elliptic fixed points at $(\varphi=\pi/2, p=0)$ and $(\varphi=3\pi/2, p=0)$ corresponding to a period-2 orbit along the minor axis with $F(\pi/2,0)=-\varepsilon^2/(1-\varepsilon^2)$.

(3) $F(\varphi,p)=0$ corresponds to the period-2 orbit along the major axis with $(\varphi=0, p=0)$ and $(\varphi=\pi, p=0)$, seen in the PSS as two hyperbolic fixed points.

The topology of the PSS (Fig. 1), is dominated by two isolated periodic orbits. The condition for stability is, according to Ref. [1],

$$\frac{\rho}{2R(\varphi)}-1\begin{cases}>0 & \text{unstable},\\ <0 & \text{stable},\end{cases} \tag{6}$$

where $R(\varphi)$ is the radius of curvature and ρ is the distance in coordinate space between two successive collisions. Using this stability criterion, we get for the periodic orbit along the long diameter $\rho/2R=1/(1-\varepsilon^2)>1$, and therefore it is unstable. In contrast, the orbit along the short diameter obeys $\rho/2R=1-\varepsilon^2<1$ and is stable.

According to Ref. [16], Poncelet's theorem on projective geometry can be applied to elliptical billiards [31]. It states that all trajectories possessing the same value of $F(\varphi,p)$ share the same caustic and the same type of dynamics. In the case of periodic orbits this means that, given one periodic orbit, with a certain value of $F(\varphi,p)$, every trajectory with the same value of $F(\varphi,p)$ is also periodic and has actually the same period. Consequently, the only isolated periodic orbits are the two discussed period-2 orbits; all the other periodic orbits are nonisolated and form families.

B. Escape rates

Let us focus now on the escape rates of a static elliptical billiard with a hole placed on its boundary. In this section we use for all simulations $A=2$, $B=1$, i.e., the numerical eccentricity $\varepsilon=\sqrt{3}/2\approx 0.87$. The number N_0 of particles in the initial ensemble is $N_0=10^7$. Each particle is propagated for at most 10^6 boundary collisions unless it escapes earlier. The initial conditions $(\varphi_0,\alpha_0)_i$, $i=1,2,\ldots,10^7$ (the index i stands for the ith particle) are chosen randomly. Note that the angle α_0 is distributed uniformly in $[0,\pi]$, not $p_0=\cos\alpha_0$. We choose two different hole positions $\varphi_\Delta=0$ and $\varphi_\Delta=\pi/2$. The hole size Δ is set to $\Delta=0.03$ (measured in φ). $\varphi_\Delta=0$ corresponds to a hole lying in the very right of the ellipse of Fig. 1, and $\varphi_\Delta=\pi/2$ corresponds to the location at the very top of the ellipse. The reason for this choice is the following. If the hole lies at $\varphi_\Delta=0$, none of the librator orbits can escape, since their invariant curves are not connected with the hole, whereas if $\varphi_\Delta=\pi/2$, all orbits can participate in the decay. In both cases, all rotator orbits can escape (as long as they are not periodic), since they are ergodic with respect to the phase space variable φ. The main data of these simulations are the numbers of remaining particles in the billiard as a function of the number of collisions $N(n)$ or the elapsed time $N(t)$. Note that we refer to $N(t)$ as the *escape rate*, as is done in the literature, whereas we will call $\dot{N}(t)$ the *emission rate*.

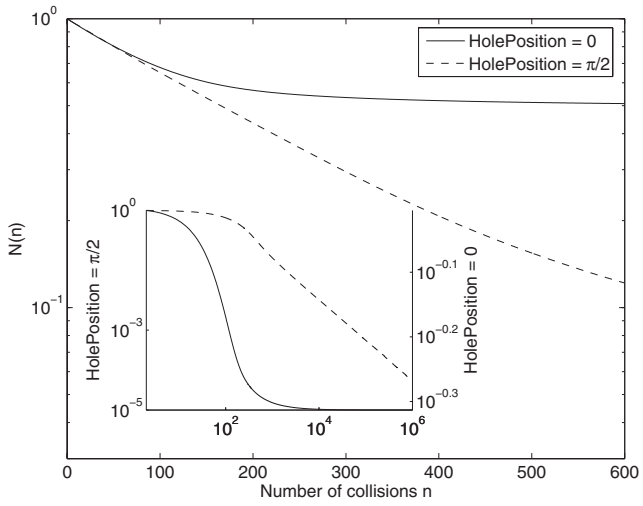

FIG. 2. Semilogarithmic plot of the escape rate; two different hole positions are shown (double-logarithmic scale in the inset).

The results of the simulations are shown in Fig. 2. Two qualitatively different behaviors of the decay are observed for the two different hole positions: (1) If $s_\Delta=\pi/2$, the fraction of remaining particles $N(n)$ as a function of the number of collisions approaches zero for $n\to\infty$. (2) If $s_\Delta=0$, $N(n)$ approaches a saturation value $N_s(\varepsilon)>0$ after roughly $n=2\times 10^3$ collisions.

The saturation value $N_s(\varepsilon)$ in the case $s_\Delta=0$ is, of course, caused by particles traveling on librators. Since the librator orbits are not connected with the hole, these particles will stay forever in the billiard. We will derive an exact expression for $N_s(\varepsilon)$ in the next section. In both cases of the hole position, the short-time behavior (Fig. 2) of the decay is exponential $N(n)\sim\exp(-\tau n)$ (roughly for the first 50 collisions in the case $s_\Delta=0$ and 300 collisions in the case $s_\Delta=\pi/2$). The decay constant τ is approximately given by $\tau\approx\Delta/2\pi$ [32]. The long-time behavior $(n>2\times 10^3)$ of $N(n)$ in the case $s_\Delta=\pi/2$ corresponds to an algebraic decay $N(n)\sim n^{-c}$, seen as a straight line in the inset of Fig. 2. This power law decay is typical for integrable systems and known in the literature (see, e.g., Ref. [5] or [33]), but there is no work discussing the case of the ellipse, except for Ref. [19], where the algebraic decay, is observed experimentally, even though not in such detail.

A heuristic model explaining this algebraic behavior is provided in [5]. The discussion given there holds for a rectangular box, where $|\boldsymbol{p}\cdot\boldsymbol{e}_n|$ ($\boldsymbol{e}_n$ is the unit vector normal to the opening) is a constant of motion. Nevertheless, the results obtained there can be easily transferred to the case of the ellipse by replacing $|\boldsymbol{p}\cdot\boldsymbol{e}_n|$ by $F(\varphi,p)$. According to [5], the fraction of remaining particles should decay for large n like $N(n)\sim n^{-1}$. The extracted value from our data is $N(n)\sim n^{-1.02}$ for $n>3\times 10^3$, i.e., in very good agreement with the analytical prediction.

C. Saturation value $N_s(\varepsilon)$

Let us now study whether the escape rates depend on the numerical eccentricity ε. Indeed, the qualitative behavior of

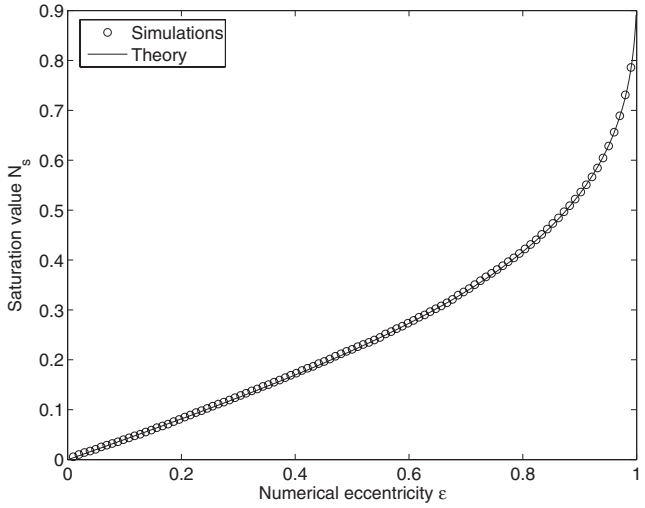

FIG. 3. Dependence of the saturation value N_s on ε.

the decay remains unchanged; only the saturation value $N_s(\varepsilon)$ is different for different values of ε for the hole at the short side of the ellipse, $s_\Delta=0$. This becomes immediately clear if one considers that ε determines the degree of deformation compared to the circle: Since in the circle there are exclusively rotator orbits, $N_s(0)$ should be zero, and with increasing ε the offset $N_s(\varepsilon)$ should increase too.

The fraction of escaped particles as a function of ε is shown in Fig. 3. One can also calculate $N_s(\varepsilon)$ from the following theoretical considerations; the result is in excellent agreement with the numerical data points (see Fig. 3).

All initial conditions corresponding to particles propagating on librators lie inside the area $A_{II}(\varepsilon)$ bounded by the separatrix of Fig. 1. We denote by $f(\varepsilon)=A_{II}(\varepsilon)/A_{PSS}$ the ratio of $A_{II}(\varepsilon)$ and the total area A_{PSS} of the phase space:

$$A_{PSS} = (p_{max} - p_{min})(\varphi_{max} - \varphi_{min}) = 4\pi. \tag{7}$$

To calculate $A_{II}(\varepsilon)$, we need an analytic expression for the curve belonging to the upper half of the separatrix, which is a function $p_{sx}(\varphi)$. Then this area is given by

$$A_{II}(\varepsilon) = 2\int_0^{2\pi} d\varphi\, p_{sx}(\varphi). \tag{8}$$

We know that for the motion along the separatrix $F(\varphi,p)=0$. Thus, we can exploit (5) and get

$$p_{sx}(\varphi) = p(\varphi, F=0) = \sqrt{\frac{\varepsilon^2}{1+(1-\varepsilon^2)\cot^2\varphi}}. \tag{9}$$

We see immediately that $A_{II}(\varepsilon)$ (8) depends on ε, and so does the saturation value. To obtain $N_s(\varepsilon)$, we have to account for the fact that the initial conditions are distributed uniformly in the α, φ and not the p, φ space. Hence,

$$\alpha_{sx}(\varphi) = \arccos[p_{sx}(\varphi)] = \arccos\sqrt{\frac{\varepsilon^2}{1+(1-\varepsilon^2)\cot^2\varphi}}, \tag{10}$$

and as a result $f'(\varepsilon)=A'_{II}(\varepsilon)/2\pi^2$, similar to (7), and $A'_{II}(\varepsilon)$ is

$$A'_{II}(\varepsilon) = 2\int_0^{2\pi} d\varphi\, \alpha_{sx}(\varphi). \tag{11}$$

The fraction of escaped particles is just $1-f'$, and the saturation number is

$$N_s(\varepsilon) = f'(\varepsilon). \tag{12}$$

In Fig. 3, perfect agreement between the analytical considerations presented above and the numerical simulations can be seen. As a consequence, varying ε allows us to control the number of particles being emitted.

III. TIME-DEPENDENT ELLIPSE

In this section, we investigate the escape rates for the time-dependent ellipse. Since the boundary transfers momentum to the particles upon collisions, their energy is not conserved any more. The collision point of a particle with the boundary is not defined by φ only, but we need additionally the time t to make the point well-defined in coordinate space, since the boundary $\mathcal{B}(t)$ depends explicitly on t. Likewise, the direction of a particle has to be described by $\boldsymbol{v}=(v_x,v_y)$ and not just by $p=\cos\alpha$, since $|\boldsymbol{v}| \neq \text{const}$. Representative visualizations of the resulting 4D phase space, like the 2D PSS for the static billiard, are difficult to achieve.

To drive the ellipse, we apply harmonic oscillations to its boundary $\mathcal{B}(t)$,

$$\mathcal{B}(t) = \{\boldsymbol{b}(\varphi,t) | \varphi \in [0,2\pi)\}, \tag{13}$$

$$\boldsymbol{b}(\varphi,t) = \begin{pmatrix} x(\varphi,t) \\ y(\varphi,t) \end{pmatrix} = \begin{pmatrix} A(t)\cos\varphi \\ B(t)\sin\varphi \end{pmatrix}, \tag{14}$$

where $A(t)$ and $B(t)$ are given by

$$A(t) = A_0 + C\sin(\omega t + \delta), \tag{15a}$$

$$B(t) = B_0 + C\sin(\omega t + \delta), \tag{15b}$$

$C>0$ is the driving amplitude, and δ is a phase shift. A_0, B_0, and C have to be chosen in such a way that $A(t)>0$ and $B(t)>0$ for all t. We refer to (15) as the *breathing ellipse*. As already done in Sec. II, we set $A_0=2$ and $B_0=1$, and use values of C between 0.01 and 0.30 only. The velocity $\boldsymbol{u}(\varphi,t)$ of the boundary and the numerical eccentricity are

$$\boldsymbol{u}(\varphi,t) = \begin{pmatrix} \omega C\cos(\omega t+\delta)\cos\varphi \\ \omega C\cos(\omega t+\delta)\sin\varphi \end{pmatrix}, \tag{16}$$

$$\varepsilon(t) = \sqrt{1 - \frac{[1+C\sin(\omega t+\delta)]^2}{[2+C\sin(\omega t+\delta)]^2}}. \tag{17}$$

A. Mapping

Just as in the static case, a discrete mapping is sufficient to characterize the full dynamics of a particle. Consequently, the trajectory of a particle consisting of N bounces is given by

$$\mathcal{C} = \{(t_0, \varphi_0, \boldsymbol{v}_0), (t_1, \varphi_1, \boldsymbol{v}_1), \ldots, (t_N, \varphi_N, \boldsymbol{v}_N)\}. \quad (18)$$

The mapping for the next collision time t_{n+1} is determined implicitly by

$$\left(\frac{v_x^n(t_{n+1}-t_n)+x_n}{A_0+C\sin(\omega t_{n+1}+\delta)}\right)^2+\left(\frac{v_y^n(t_{n+1}-t_n)+y_n}{B_0+C\sin(\omega t_{n+1}+\delta)}\right)^2-1=0, \quad (19)$$

where, for a given t_n and φ_n, x_n and y_n are calculated from (14) and t_{n+1} is defined by the smallest $t_{n+1}>t_n$ that solves (19). The next collision point is given by $\boldsymbol{x}_{n+1}=\boldsymbol{x}_n+\boldsymbol{v}_n(t_{n+1}-t_n)$, and φ_{n+1} can be obtained by inverting (14). Once (t_{n+1}, φ_{n+1}) is determined, the next velocity $\boldsymbol{v}_{n+1}$ is given by

$$\boldsymbol{v}_{n+1} = \boldsymbol{v}_n - 2[\hat{\boldsymbol{n}}_{n+1}\cdot(\boldsymbol{v}_n - \boldsymbol{u}_{n+1})]\cdot\hat{\boldsymbol{n}}_{n+1}, \quad (20)$$

where the boundary velocity $\boldsymbol{u}_{n+1}$ is given by (16) and the normal vector by $\hat{\boldsymbol{n}}_{n+1}=\hat{\boldsymbol{n}}'_{n+1}/|\hat{\boldsymbol{n}}'_{n+1}|$, $\hat{\boldsymbol{n}}'_{n+1}=(-B(t_{n+1})\cos\varphi_{n+1}, -A(t_{n+1})\sin\varphi_{n+1})^{\mathrm{T}}$.

The maximal velocity change of a particle upon a single collision with the boundary according to Eq. (20) is $\Delta|\boldsymbol{v}|=\pm 2\omega C$. Thus, it can happen that the particle undergoing a boundary collision at the time t' is not reflected, in the sense that the sign of the velocity component normal to the boundary tangent is not reversed; the particle continues traveling outside $\mathcal{B}(t')$, but of course still inside $\mathcal{B}(t>t')$. This is the case if the ellipse is expanding and $u_n<v_n<2u_n$ holds, where v_n and u_n are the normal components of the particle and the boundary velocity before the collision. As a consequence, the angle α between the tangent $\boldsymbol{t}$ and the velocity $\boldsymbol{v}$ is not restricted to the interval $[0,\pi]$ as it was in the case of the static ellipse, but now $\alpha\in[-\pi,\pi]$. Upon such collisions with the expanding boundary, the particles are always slowed down, they lose energy [34,35]; whereas upon collisions with the contracting ellipse they gain energy.

B. Escape rates

We focus on the case $s_\Delta=0$, in order to examine the effect of the driving on the number of particles in the billiard. For the static case, the saturation value was caused by the librator orbits (see Sec. II C). We assume that these librator orbits will be deformed or partially destroyed by the driving, leading to a nonvanishing decay even for large times. On the other hand, we expect no stabilization of the rotator orbits, i.e., no deformation in a way that they will not escape. All periodic orbits become unstable when applying the driving, and in Ref. [25] it was concluded that it is impossible to trap unstable periodic orbits in the ellipse via boundary oscillations. Note that this is not true in general for driven systems; unstable periodic orbits can be stabilized by a driving force, e.g., in the Kapitsa pendulum [36].

We consider two different borderline cases: $|\boldsymbol{v}_0|\approx\omega C$ [intermediate-velocity ensemble (IVE)] and $|\boldsymbol{v}_0|\gg\omega C$ [high-velocity ensemble (HVE)]. In the first case, the velocity has the same order of magnitude as the boundary velocity. This leads to a momentum transfer (maximal $2\omega C$) of the same order of magnitude compared to the initial momentum, and we expect significant changes in the dynamics. In the second case, the particles move much faster than the boundary; consequently the momentum transfer will be very small, and the dynamics will be similar to that of Sec. II. Naturally, it would also be interesting to examine the case $|\boldsymbol{v}_0|\ll\omega C$. However, the first few collisions then accelerate the particles to velocities $|\boldsymbol{v}|\approx\omega C$ and, after a short time, we encounter the situation of the first case. The parameters of the simulations are $N_0=10^5$, $\omega=1$, $C=0.01, 0.05, 0.10, 0.15, 0.20, 0.25, 0.30$, and $\delta=0$. To ensure that all the particles move inside the billiard, we let them start on the smallest ellipse (for a given C); the initial position φ_0 and the initial angle α_0 are chosen randomly. The initial velocity $\boldsymbol{v}_0$ is given by $\boldsymbol{v}_0=(\cos\alpha_0, \sin\alpha_0)$ (IVE) and $\boldsymbol{v}_0=100(\cos\alpha_0, \sin\alpha_0)$ (HVE), respectively. The fraction of remaining particles $N_C(t)$ as a function of time for different amplitudes C is shown in Figs. 4 (IVE) and 5 (HVE).

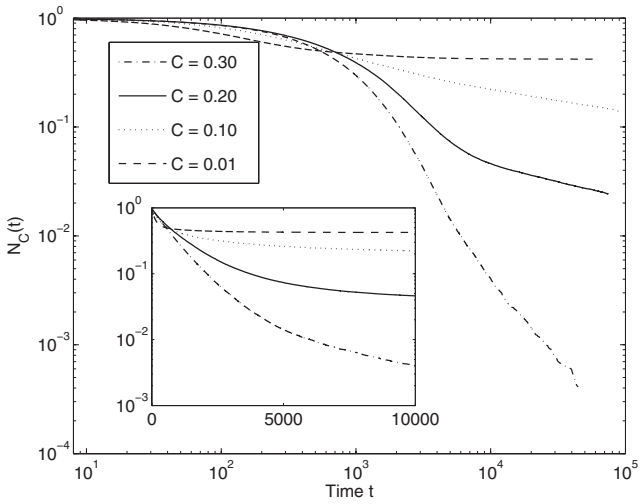

FIG. 4. Fraction of remaining particles in the IVE as a function of time for different values of the amplitude C (semilogarithmic plot in the inset).

First, we describe the behavior of the IVE. We observe a short but fast decay ($t<500$), followed by a transient (500

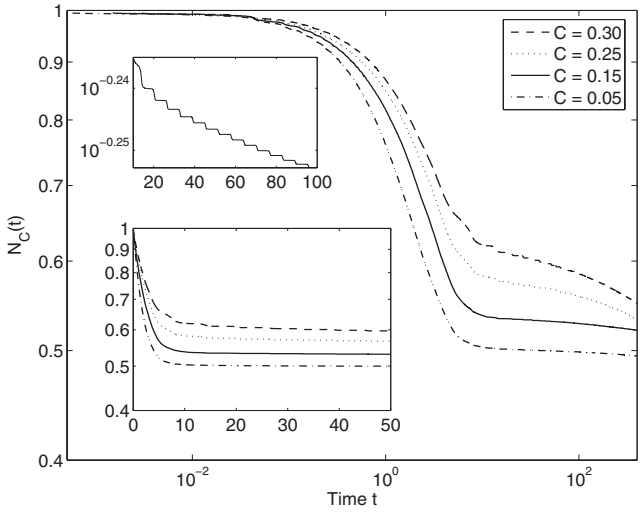

FIG. 5. Same as Fig. 4 for the HVE; additionally 2π-periodic oscillations of the decay are shown in the inset.

$<t<5000$) in which the decay slows down; and for $t>5000$, the decay is much slower than the initial fast decay for all values of C. At $t=10^4$, the values of the fraction of remaining particles are ordered according to the driving amplitudes; the lower C is, the higher is $N_C(t=10^4)$, i.e., $N_C(t=10^4)$ depends monotonically on the amplitude C. For $t>10^4$, $N_C(t)$ does not stay constant, but is still decreasing. The absolute value of the emission rate $\dot{N}_C(t)$ is larger the larger C is. This can be seen nicely in the double-logarithmic plot of Fig. 4. For values of t between 10^4 and 10^5, we encounter approximately an algebraic decay $N_C(t)\sim t^{-w}$ (we remark that this algebraic decay has been numerically shown to exist for much longer times than illustrated in Fig. 4), where the decay constant w increases monotonically with increasing C (this fact is based not only on the four values of the driving amplitude C shown here, but on simulations carried out for 20 values of C between 0.01 and 0.30).

The subdivision of the behavior, into fast initial decay–transition period–slow (near algebraic) decay, is even more pronounced in the case of the HVE (see the inset of Fig. 5). An exponential decay for small values of t slows down at around $t\approx 5$ and the fraction of remaining particles seems to approach a constant value. From Fig. 5, however, we see that the fraction of remaining particles decays for $t>10$ roughly according to an algebraic decay (at least for small values of the driving amplitude) $N(t)\sim t^w$, with a decay constant w. If we compare the fraction of remaining particles at $t=50$ for different values of the amplitude (inset of Fig. 5), we see that they are monotonically ordered according to the driving amplitudes. Surprisingly, most of the particles remain within the billiard in the case of the largest driving amplitude $C=0.30$ and the smallest fraction remains in the case of the smallest amplitude $C=0.05$. The explanation of this effect is provided later, in Sec. IV, when we examine the dependence of the PAM $F(\varphi,p)$ on the driving.

In the inset of Fig. 5, a modulation of the escape rate with period $T=2\pi$ can be seen, being exactly the period of the applied driving law (14). Specifically, for $t\geqslant 10$, where all particles starting on rotator orbits have already escaped, $N_C(t)\approx$ const during approximately 11/12 (empirically observed) of one period and subsequently $\dot{N}_C(t)\neq 0$ during a time interval $T/12$ only. From this behavior, it is evident that the ellipse operates from a certain time on as a pulsed source of particles. These repeated intervals are centered around points t_m of maximal extension of the ellipse, $t_m=(4m+1)\pi/2$, $m=2,3,4,\ldots$. During the expansion period, dominantly vertical but also horizontal processes turn librators into rotators. The moving ellipse remains for a comparatively long time period in the vicinity of the extremal configuration at t_m and consequently the newly created rotators escape. Therefore, the dynamics is effectively probed during these short time intervals centered around t_m. During the contraction period, the librators are stabilized via vertical processes; consequently $\dot{N}_C(t)\approx 0$ during 11/12 of a period T.

C. Mechanisms for the destruction of the librators

In the driven ellipse, librators can escape from the billiard, whereas this is not the case for the static ellipse. There are two fundamental processes that perturb or even completely destroy the librator orbits (unprimed variables denote the static, whereas primed ones describe the driven system).

(1) *Vertical process*. The angle of incidence of a collision does not coincide with the reflection angle because of a change of momentum due to the motion of the boundary of the ellipse. In phase space, the momentum then undergoes a certain change Δp upon a collision and the particle moves vertically in the PSS.

(2) *Horizontal process*. A particle that would hit the boundary at a certain point φ hits the boundary in the driven case at φ', simply because the ellipse's boundary has moved, whereas p stays nearly unchanged. This corresponds to a horizontal move in the PSS.

These processes are fundamental in the sense that every change ΔF can be decomposed [at least for small changes $(\Delta\varphi,\Delta p)$] into $\Delta F=\Delta F_h+\Delta F_v$, where $\Delta F_{h,v}$ denote the individual changes caused by the horizontal and the vertical process, respectively.

In general, these effects do not appear isolated, but a combination $(\Delta\varphi,\Delta p)$ of both will occur in a single collision. We can compare the orbits (φ_i',p_i') of the driven ellipse to the corresponding ones of the static ellipse (φ_i,p_i) by considering the quantity $F(\varphi,p)$ [see Eq. (5)]. In contrast to the case of the static ellipse where $F(\varphi_i,p_i)=\text{const}\,\forall\, i$, we have $F(\varphi_i',p_i')\neq F(\varphi_j',p_j')$ $(i\neq j)$ for the driven case, i.e., F is no longer a constant of motion. The difference ΔF (see Fig. 1) upon a collision is a measure of whether a librator approaches the separatrix $(\Delta F>0)$ or whether it moves in phase space toward the position of the elliptic fixed points $(\Delta F<0)$ of the static case. An increase with respect to F reflects the dependency of "moving" in phase space from confined librator to escaping rotator orbits.

1. Vertical processes

To isolate this effect, we examine a particle that hits the boundary at $\varphi=\pi/2$ under a certain angle α in the static case. The velocity of the particle can be written as $\boldsymbol{v}_0=(-v\cos\alpha, v\sin\alpha)$, $v=|\boldsymbol{v}_0|$. In the driven ellipse, we will assume that the particle hits the boundary in the neutral position $[A(t)=A_0, B(t)=B_0]$, so we have $\varphi'=\varphi=\pi/2, \Rightarrow \Delta\varphi=0$. The boundary velocity $\boldsymbol{u}(\varphi,t)$ of the ellipse is maximal at this configuration and has a vertical component only, $u_n=u_y=\pm\omega C$, depending on whether the ellipse is expanding "+" or contracting "−." The velocity of the particle at the next collision in the static case is $\boldsymbol{v}_1=(-\cos\alpha,-\sin\alpha)^{\mathrm{T}}$ and hence $p_1=p_0=\cos\alpha$. The corresponding velocity in the driven case is $\boldsymbol{v}_1'=(-v\cos\alpha,-v\sin\alpha\pm 2\omega C)^{\mathrm{T}}$. Now, $p_0'=p_0\neq p_1'$, since

$$p_1'=\underbrace{\frac{\cos\alpha}{\sqrt{1\mp\frac{4\omega C}{v}\sin\alpha+\frac{4\omega^2C^2}{v^2}}}}_{f}. \tag{21}$$

If the ellipse is contracting (+ sign in the factor f), $p_1'=\cos\alpha/f$ is smaller than $p_1=\cos\alpha$ because $f>1$, i.e., $\Delta p<0$ $(p_1'=p_1+\Delta p)$. In phase space the particles moves toward

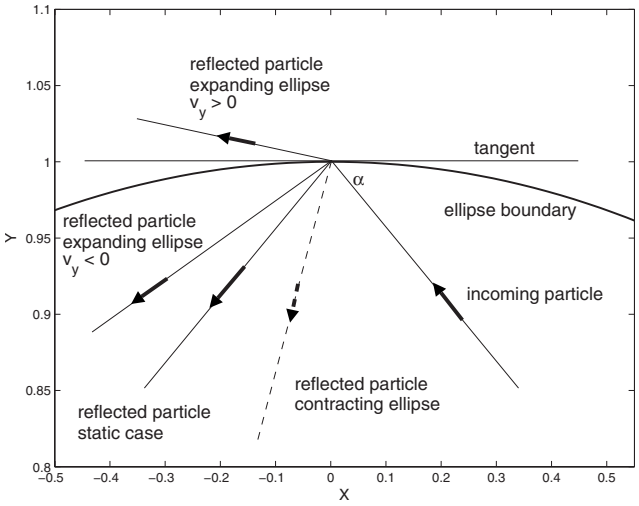

FIG. 6. Vertical process in coordinate space.

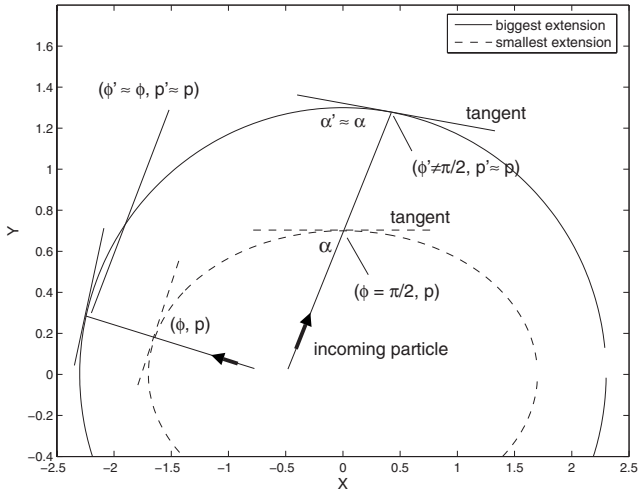

FIG. 8. Horizontal process in coordinate space.

the elliptic fixed points, which does not lead to the destruction of the librators. If the ellipse is expanding ($-$ sign in the factor f), Δp will be larger than zero if $f<1$. This is equivalent to

$$\sin \alpha > \frac{\omega C}{v}, \tag{22}$$

and since $v_n = v \sin \alpha$ and $u_n = \omega C$ Eq. (22) is equivalent to $v_n > u_n$, which is a necessary condition for a collision to take place. If additionally to Eq. (22) $\sin \alpha < 2\omega C/v$, then $v_n = v_y > 0$ and thus $\alpha' < 0$ (see Fig. 6); the particle is not reflected in the sense that the sign of v_n is not reversed. For $\sin \alpha > 2\omega C/v$, it follows that $v_n = v_y < 0$; the particle is reflected. In both cases $\Delta p > 0$, the particle moves toward or even beyond the separatrix; in the latter case, the librator has changed into a rotator. This process can therefore lead to the destruction of the librator orbits. In Figs. 6 and 7, the process is shown in coordinate as well as in phase space. This process happens for any value of φ; nevertheless, the case $\varphi \approx \pi/2$ is especially important for two reasons: (1) The absolute value of the change Δp is largest for $\cos \alpha \approx \sin \alpha$; for particles on librators this is approximately true if $\varphi \approx \pi/2$. (2) For a constant Δp, the corresponding $\Delta F(\varphi, p)$ is largest for $\varphi = \pi/2$, because the vertical spacing of the invariant curves is smallest at $\varphi = \pi/2$. Consequently, the horizontal processes that contribute the most to changing a librator into a rotator occur mainly around $\varphi \approx \pi/2$ (and $\varphi \approx 3\pi/2$ because of symmetry).

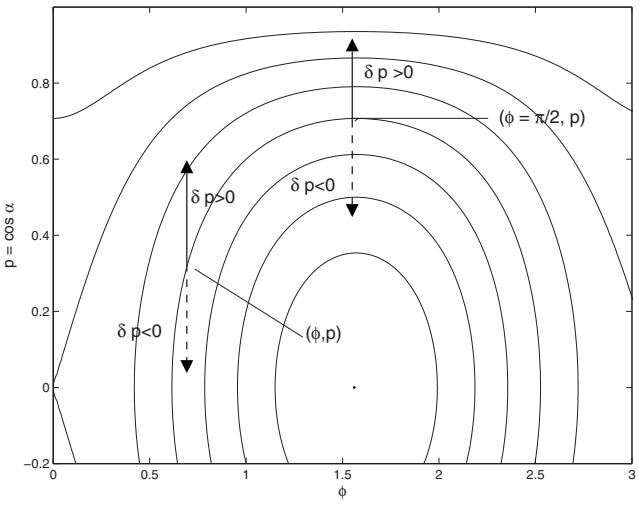

FIG. 7. Vertical process in phase space.

2. Horizontal processes

We consider a particle that starts moving in a static ellipse corresponding to the smallest possible ellipse (given a certain amplitude) in the driven case, hitting the boundary of this static ellipse at $\varphi = \pi/2$ under a certain angle α (see Fig. 8). We choose all the parameters such that the particle will hit the boundary of the driven ellipse at the time t' at the position $\varphi' \neq \varphi$, when the boundary $\mathcal{B}(t')$ has its maximal extension. The new angle α' is approximately equal to α (see Fig. 8). This rough estimate becomes better with increasing α and decreasing distance between the two ellipses; thus $\Delta p \approx 0$, i.e., the particle moves horizontally in the PSS (see Fig. 9). To calculate φ' or $\Delta\varphi$ as a function of C and α is very tedious and the exact result is not very helpful. We therefore restrict ourselves to an approximation and linearize the boundary of the ellipse locally at $\varphi = \pi/2$. The collision point on $\mathcal{B}(t)$ is

$$\varphi' = \arctan \frac{y}{x} \approx \arctan \frac{(2+C)\tan \alpha}{2C}. \tag{23}$$

In general, we have to respect the sign of x and y to obtain φ' from (23). $|\Delta\varphi| = |\varphi' - \varphi|$ depends sensitively on α and decreases with increasing α. $|\Delta\varphi|$ is largest for $\varphi \approx \pi/2$, since α there reaches its minimal value for the librator orbits. The sign of the corresponding change ΔF depends on the sign of $\Delta\varphi$ and the quadrant in which φ lies (e.g., for $\Delta\varphi < 0$, $\Delta F > 0$, if φ lies in the second or fourth quadrant). There is no obvious region with respect to φ where the destruction of the librators mainly occurs, since two opposite effects balance each other: (1) The absolute value of the change $|\Delta\varphi|$ is

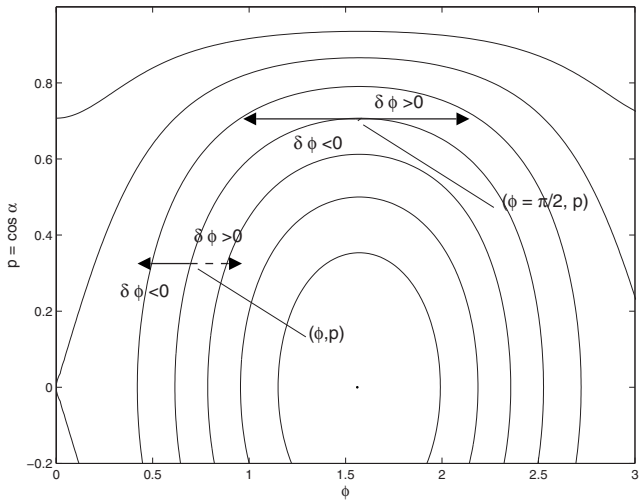

FIG. 9. Horizontal process in phase space.

largest for $\varphi \approx \pi/2$. (2) Given a certain $\Delta\varphi$, the corresponding changes ΔF increase with increasing distance between φ and $\pi/2$, because the horizontal spacing of the invariant curves is smallest there (see Fig. 9). Nevertheless, the position $\varphi=\pi/2$ (and $\varphi=3\pi/2$) is in a way exceptional: any change $\Delta\varphi$, independent of the sign, results in a change $\Delta F>0$, leading to a destruction of the librators.

D. Qualitative model of the decay

We isolated two processes that are able to change $F(\varphi,p)$ in the course of the dynamics. Particles on librator orbits are scattered upon boundary collisions either toward the elliptic fixed points or toward or even beyond the separatrix. For a single particle, such a scattering process happens at every collision, and the effective change ΔF after a certain time depends on the sequence of these processes; hence $\Delta F = \Delta F_1 + \Delta F_2 + \cdots + \Delta F_n$ after n collisions. This effective change in $F(\varphi,p)$ is very difficult, if not impossible, to predict, since each individual change ΔF_i depends on four parameters already: (1) the absolute value $|\boldsymbol{v}_i|$ of the particle velocity, (2) the angle α_i of the velocity with the boundary, (3) the location φ_i of the collision point on the boundary, and (4) the time t_i which determines the position of the boundary and the boundary velocity $\boldsymbol{u}_i(t_1)$ of the ellipse (these four parameters are of course just the variables of the four-dimensional discrete mapping; see Sec. III A). Now we consider not only a single particle, but an ensemble of N particles with initial conditions $(\varphi_j,\boldsymbol{v}_j)$, $j=1,2,\ldots,N$. The effective change $(\Delta F)_j$ (where the index j indicates the jth particle) after n collisions can vary significantly from particle to particle, since the sequence of these four parameters will be very different for each individual particle. Each of the N sequences is governed by applying the discrete mapping of Sec. III A n times on each initial condition $(\varphi_j,\boldsymbol{v}_j)$. The underlying nonlinear dynamics of this discrete mapping and the fact that all particles start from different initial conditions lead to such unique sequences, and will consequently cause large fluctuations in the effective ΔF and accordingly large fluctuations in quantities that depend on $F(\varphi,p)$. In the following, a qualitative explanation of the escape rates $N_C(t)$ (decay) of the IVE and the HVE is given.

We focus on the HVE first. The initial fast decay of the number of particles ($t<5$) is due to the rotator orbits that are connected with the hole and escape very rapidly. Additionally, some of the particles starting on librator orbits near the separatrix $F \lesssim 0$ contribute. The longer-time decay ($t>10$) is caused by particles starting on librators that have been scattered across the separatrix. The closer an orbit of a particle lies to the elliptic fixed points, the longer it takes until the effective change ΔF is big enough to reach the separatrix ($F=0$). From Eqs. (21) and (23) it follows that the individual changes ΔF_i under a single collision increase with increasing amplitude C. This explains the increasing emission rate $\dot{N}_C(t)$ with increasing C, since at a given time t the number of particles that can participate in the decay is larger for larger values of C. The decay in the transient region ($5<t<10$) is caused by a superposition of the tail of the initial fast decay (roughly exponential) and the onset of the slow (roughly algebraic) decay.

With very similar arguments, the decay of the IVE can be explained qualitatively. Since the velocity of the particles and the velocity of the boundary are of the same order of magnitude, the changes ΔF are much larger compared to those of the HVE. This leads to a very early onset of the slow (algebraic) decay; consequently the transient region is broadened.

IV. ANGULAR MOMENTUM

To validate the qualitative model of Sec. III D, we investigate the PAM $F(\varphi,p)$ further. The contours of $F(\varphi,p)$ are shown in Fig. 1; depending on the initial value of F, particles move on rotator or librator orbits (see Sec. II A).

Throughout the following sections, we analyze properties such as the escape time for an ensemble of particles possessing certain initial distributions in, e.g., phase space or the PAM F. We emphasize that in the case of the distribution of the F values we always refer to the initial distributions of F at $t=0$ [37].

A. Escape time versus initial conditions in phase space

As an example, the escape time as a function of the starting points in phase space is shown in Fig. 10 ($C=0.10$, IVE), i.e., we assign to each initial condition (φ_0,p_0) (10^5 particles) an escape time. Large values of the escape time correspond to initial conditions belonging to librator orbits lying around the elliptic fixed points at $(\varphi=\pi/2,p=0)$ and $(\varphi=3\pi/2,p=0)$. On the other hand, initial conditions corresponding to small values of the escape time lie around areas that correspond to the rotator orbits. Overall, the results of Fig. 10 are in good agreement with our predictions of Sec. III D, where we derived large escape times for particles with initial conditions close to the two elliptic fixed points and short escape times for particles starting on librator orbits.

B. Escape time versus initial angular momentum

In this section, we investigate the escape time t_{esc} versus the initial angular momentum $F(\varphi_0,p_0)$ of the corresponding

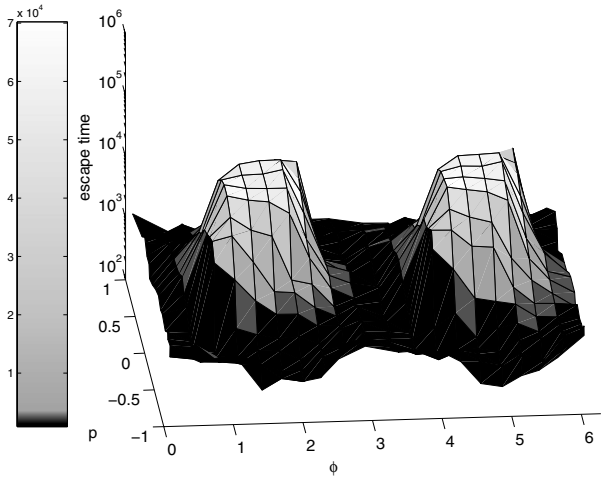

FIG. 10. Escape time versus initial conditions in phase space for $C=0.10$ (IVE). The escape time is largest for initial conditions close to the elliptic fixed points.

ensemble of particles in phase space for different amplitudes C. We consider escaped particles only.

The results for the IVE are shown in Fig. 11. For small escape times $t_{esc} \lesssim 10$, there is a narrow, serpentine chain in which all the pairs (t_{esc}, F) lie. Only pairs with $F>0$ corresponding to rotators occur for $t_{esc} \lesssim 10$. We will explain this below in the course of the discussion of the HVE. Apart from this narrow, serpentine chain, the values of the escape times for $F>0$ are scattered mainly over a rectangular area with $10 \lesssim t_{esc} \lesssim 10^4$. This area becomes wider in t with increasing C: $10 \lesssim t_{esc} \lesssim 10^3$ corresponds to $C=0.01$ and $10 \lesssim t_{esc} \lesssim 10^4$ corresponds to $C=0.10$. These are the particles that are associated with the initial fast decay. The widening of this area can be explained with our model from Sec. III D. In the case $C=0.01$ (inset of Fig. 11), the particles with $F>0$ escape, similarly to the static case with an exponential rate, and after a certain time, e.g., $t_{esc} \approx 1000$, most of them have escaped.

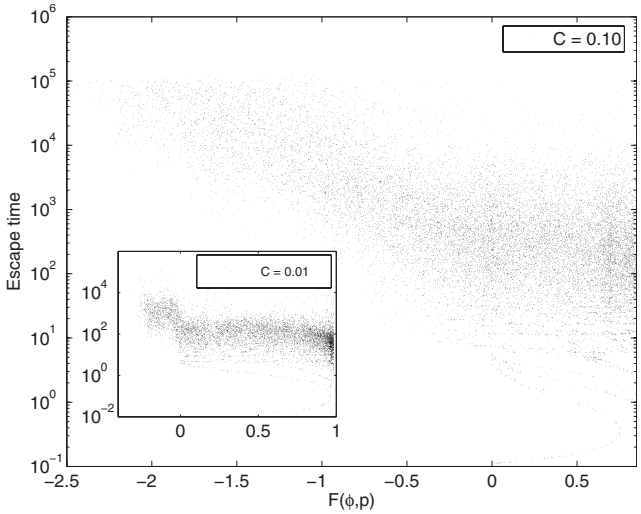

FIG. 11. Escape time versus initial angular momentum $F(\varphi_0, p_0)$ ($F=0$ corresponds to the separatrix in the static ellipse and $F=-3.1$ to the elliptic fixed points) in the IVE for $C=0.10$ and 0.01 (inset).

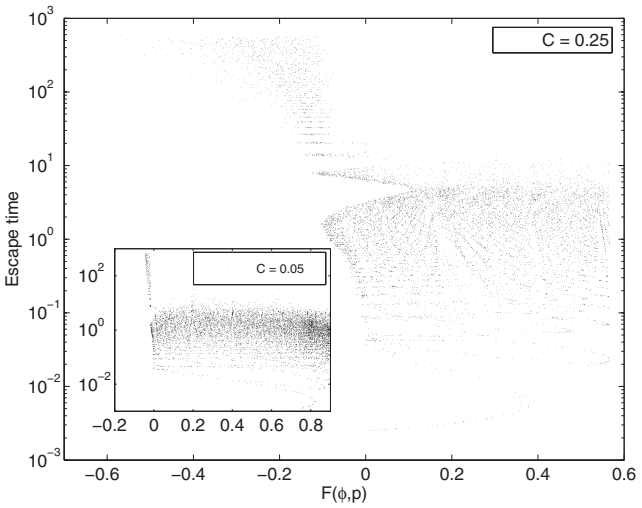

FIG. 12. Same as Fig. 11 for the HVE, $C=0.25$ and $C=0.05$ (inset).

Consequently, the algebraic decay establishes itself (see Fig. 4). With increasing amplitude, horizontal and vertical processes lead to larger changes ΔF. Due to multiple separatrix-crossing scattering the available range in the time t to escape clearly becomes larger. The appearance of rather high densities at $F \approx 0.9$ and $F \approx 0$ in Fig. 11 and at $F \approx 1$ in the inset is explained below, in Sec. IV C.

For values of $F<0$, corresponding to librator orbits, the values of the escape time are grouped in an inclined band, i.e., for smaller values of F, the escape time is on average higher. In the case $C=0.01$, the band stops at $F \approx -0.20$; orbits with smaller initial values of F just did not escape until 5×10^4 collisions were reached. For $C=0.10$, this band covers almost the hole range in F, due to the larger driving amplitude and the larger effective changes ΔF.

In Fig. 12, the results of the HVE are shown. We can match perfectly the exponential short-time behavior and the algebraic tail with the two major areas in the picture. All particles with initial values $F>0$, corresponding to rotator orbits, have escape times of $t_{esc}<10$, whereas particles on librator orbits with initial values of $F<0$ possess escape times $t_{esc}>10$. Due to high particle velocities, the effects of the horizontal and vertical processes are rather small; it takes around $t \approx 10$ (corresponds to approximately 500 collisions) until the first librators are destroyed. Up to 2.5×10^4 collisions, only particles with $F \gtrsim 0$ escaped ($C=0.05$), whereas for $C=0.25$ particles with $F \gtrsim -0.5$ decayed.

For values $F<0$ and $t_{esc}>10$ horizontal, narrow layers can be observed in Fig. 12. The vertical spacing of these layers is 2π, which is again the period of the breathing ellipse. The mechanism at work is the previously mentioned one (Sec. III B): When the ellipse is expanding, librators are turned into rotators, which can then escape, whereas during the contraction period, the rotators are stabilized.

As an example, the average escape time as a function of the initial value of F is shown in Fig. 13 for $C=0.10$ and the IVE. Starting from F around -2, the escape time is decreasing with increasing F, until the separatrix ($F=0$) is reached. For values of F bigger than zero, corresponding to rotators,

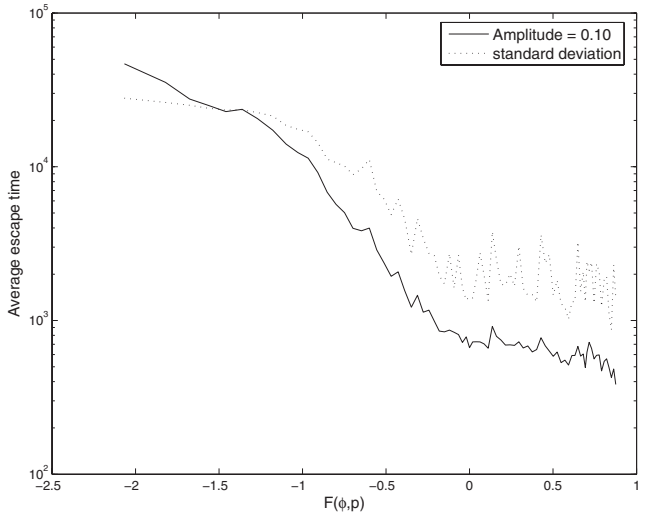

FIG. 13. Average escape time and standard deviation in the IVE as a function of the initial value of $F(\varphi_0,p_0)$ for $C=0.10$.

the escape time stays approximately constant. Nevertheless, the escape time for a single trajectory with a certain initial value F can deviate significantly from the curve shown in Fig. 13, since the standard deviation, also shown in Fig. 13, is quiet large, especially for values of $F>0$.

C. Density distributions of the escaping/ and nonescaping PAM

The choice of the initial conditions described in Sec. III B leads to an amplitude-dependent, nonuniform distribution in the density $\rho(F(\varphi_1,p_1))$ after the first collision at (φ_1,p_1). In Fig. 14, the density distribution of the initial values of $F(\varphi,p)$ for $C=0.01$ and 0.10 is shown (IVE). The three different curves in each of the figures correspond to the initial $(t=0)$ [37] density distribution of $F(\varphi,p)$ of the whole ensemble, to the initial density distribution of F for the escaped particles, and to the density distribution of F for the remaining (i.e., nonescaped) particles:

$$\rho_{all}(F_0)=\rho_{rem}(F_0)+\rho_{esc}(F_0), \quad \int_{F_{min}}^{F_{max}}\rho(F_0)dF_0=1. \tag{24}$$

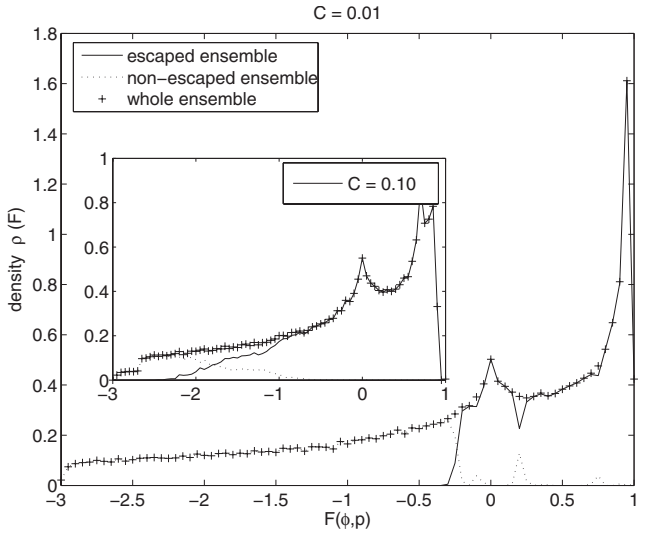

FIG. 14. Density distribution of $F(\varphi_0,p_0)$ in the IVE of the whole, the escaped, and the remaining ensemble for $C=0.01$ and 0.10 (inset).

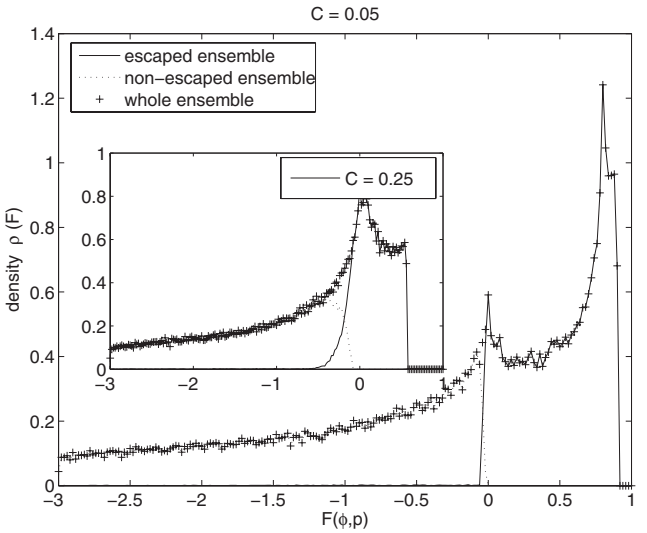

FIG. 15. Same as Fig. 14 for the HVE; $C=0.05$ and 0.25 (inset).

If we compare these figures with Fig. 11, there is a perfect correspondence between the peaks of the initial density distribution of $F(\varphi,p)$ and the high-density regions in Fig. 11, i.e., the high-density regions are due to the nonuniformity of the distribution of the initial values of F.

With increasing amplitude, the available range of initial values of F still making to an escape of the particles possible becomes larger; for $C=0.01$ only particles with $F_0\gtrsim -0.3$ escaped, whereas for $C=0.10$ already particles with initial $F_0\gtrsim -2.4$ escaped.

The results for the HVE are very similar (see Fig. 15). The main difference is that, due to the small effect of a single scattering process, the transition between escaping and nonescaping particles in F space is much sharper and shifted toward higher values of F compared to the IVE. Furthermore, the density distribution of the initial values of F explains the reverse ordering of $N_C(t=50)$ observed in Sec. III B. For $C=0.05$, due to our definition of the initial ensemble at the innermost ellipse boundary, there are many more particles with initial values $F\lesssim 1$ than in the case $C=0.25$. Overall, the fraction of particles starting on rotator orbits in the case $C=0.05$ is larger than in the case 0.25, and these rotators will escape fast.

V. VELOCITY

In the static ellipse (see Sec. II), there are two constants of motion. One is the product of the angular momenta around

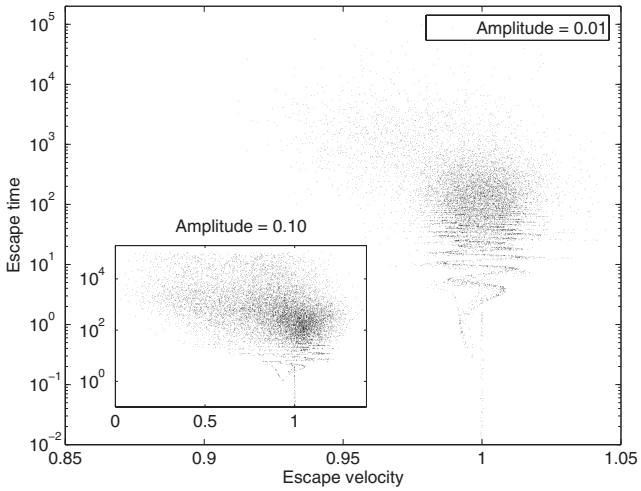

FIG. 16. Escape time versus the absolute value of the escape velocity in the IVE for $C=0.01$ and 0.10 (inset); each point corresponds to a pair $(|\boldsymbol{v}(t_{esc})|, t_{esc})$.

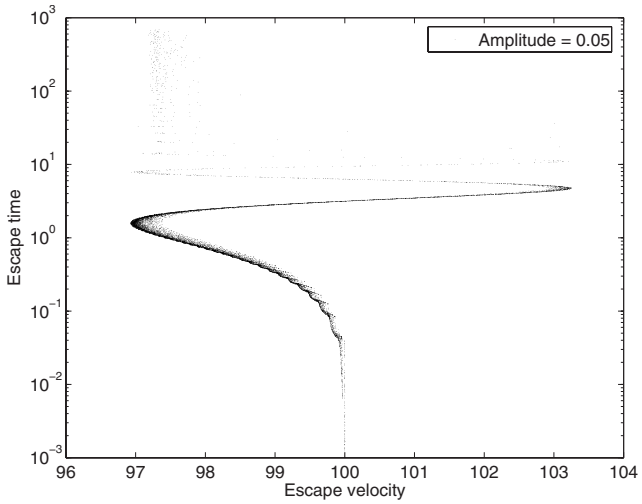

FIG. 17. Same as Fig. 16 for the HVE; $C=0.05$.

the two focus points $F(\varphi,p)$, which we just studied in the context of the driven ellipse in the previous section; the other is the energy. Since the potential is constant inside the ellipse, it is sufficient to consider the kinetic energy only. The energy of a single particle in the ellipse is given by $E_{total}=E_{kin}=m\boldsymbol{v}^2/2$. Energy conservation in the static ellipse thus means $|\boldsymbol{v}|=$const. Since all particles have the same mass it is sufficient to consider $|\mathbf{v}|$ instead of E_{total}.

When examining $F(\varphi,p)$, it is instructive to calculate F from the initial conditions (φ_0,p_0). Doing the same in the case of the velocity $|\boldsymbol{v}(t)|$ is meaningless, since we know $|\boldsymbol{v}(0)|=1$ (IVE) or $|\boldsymbol{v}(0)|=100$ (HVE) for all particles. Instead, we consider the velocity of the particles when they are actually escaping, i.e., $|\boldsymbol{v}(t_{esc})|$, the escape velocity.

A. Escape velocity versus escape time

In Fig. 16 distributions of escape times as functions of the escape velocity are shown for $C=0.01$ and 0.10. A point for every pair $(|\boldsymbol{v}(t_{esc})|, t_{esc})$ is plotted in the plane and only escaped particles are considered (IVE). At $|\boldsymbol{v}|=1$, there is a vertical line for $t\lesssim 4$. This line corresponds to the particles that escape from the billiard without a single boundary collision and thus possess an unchanged energy. For times $t\lesssim 10^2$, the pairs $(|\boldsymbol{v}(t_{esc})|, t_{esc})$ lie on a narrow serpentine band. The vertical spacing, i.e., the period of the band, is approximately 2π, which is the period of the driven ellipse. The band structure is much more pronounced in the case of the HVE (see Fig. 17), where it dominates the overall distribution, naturally emanating from $|\boldsymbol{v}|=100$. This correlation between the escape time and the escape velocity for small values of t_{esc} can be explained in the following way. The ellipse starts at $t=0$ from its neutral position with an expanding motion. As long as the ellipse is expanding, each time a particle hits the boundary it loses energy and its velocity is reduced. Since the particles move very fast compared to the motion of the boundary (HVE), they accumulate a lot of collisions until the ellipse reaches its maximal extension and starts contracting. The more collisions a particle cumulates during the expansion period, the bigger is the total energy loss. The ellipse reaches its turning point at $t=\pi/2$, i.e., every particle with an escape time $t_{esc}\leqslant\pi/2$ will have an escape velocity $|\boldsymbol{v}(t_{esc})|\leqslant|\boldsymbol{v}_0|=100$. From $t=\pi/2$ on, the corresponding escape velocities will increase until $t_{esc}=3\pi/2$ is reached, since the ellipse is contracting during this time period and every collision with the boundary will increase the energy of the reflected particle. This process is continued until all rotators have escaped, which is the case at $t\approx 10$. This explanation holds for the HVE. Since in the case of the IVE the particle velocities are similar to the boundary velocity, this effect is much less pronounced. Nevertheless, it is still visible and mainly due to orbits with initial values $F\approx 1$, since these orbits skip along the ellipse, accumulating many boundary collisions within a short period of time. The main difference between the distributions of the escape time for the two ensembles investigated above is that in the case of the HVE all rotator orbits lie on the serpentine band, whereas in the case of the IVE only rotators far away $(F\approx 1)$ from the separatrix contribute.

For intermediate times $10^2\lesssim t_{esc}\lesssim 10^3$ (IVE), the corresponding escape velocities lie closely around one for $C=0.01$ (see Fig. 16). Since the driving amplitude is very small in this case, the energy of the particles is not much changed. For larger escape times, the values of $|\boldsymbol{v}(t_{esc})|$ are a little bit more scattered, since the particles accumulated several boundary collisions, resulting in an effective change of $|\boldsymbol{v}(t_{esc})|$; still, the values deviate no more than 10% from the the initial value $|\boldsymbol{v}|=1$. As expected, the distribution of the values of $|\boldsymbol{v}(t_{esc})|$ is broadened for larger values of the driving amplitude C [see inset of Fig. 16 $(C=0.10)$], but the energy gain remains bounded, $|\boldsymbol{v}(t_{esc})|\lesssim 3$ even for $C=0.30$ (not shown here).

In the HVE, for escape times higher than 10, corresponding to particles starting originally on librator orbits, almost all escape velocities are smaller than the initial velocity $|\boldsymbol{v}_0|=100$. Horizontal and vertical processes can scatter a particle moving on a librator orbit onto a rotator orbit (and vice versa), which is a necessary condition for escaping. In which

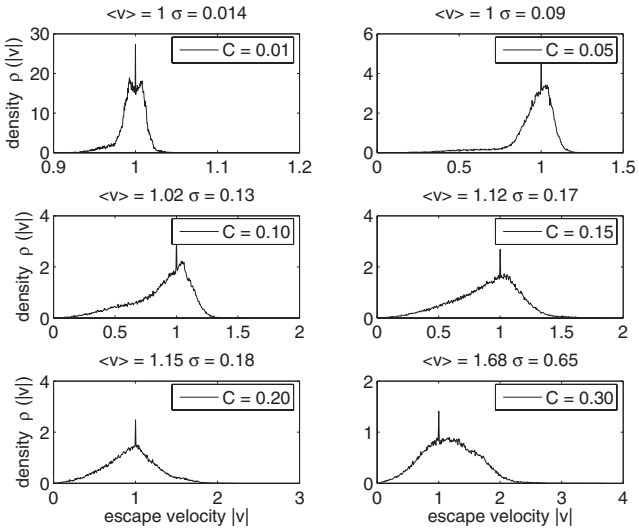

FIG. 18. Distribution of the escape velocity in the IVE for different values of C.

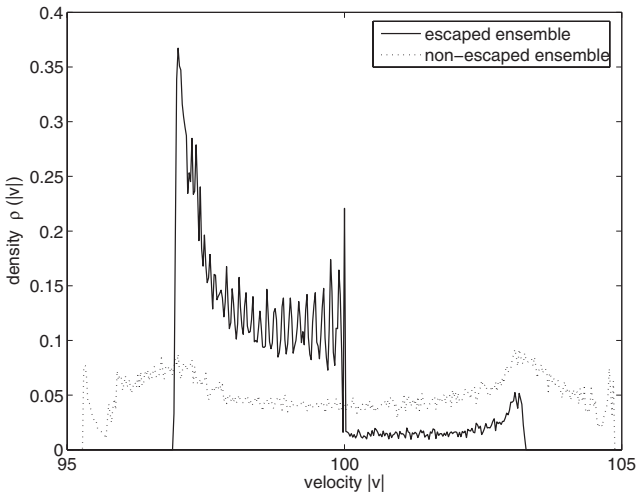

FIG. 19. Distribution of the escape velocity for the HVE; $C=0.05$.

direction (toward or away from the elliptic fixed points) a particle is scattered depends on many parameters (see Sec. III C), but at least the vertical process scatters particles during the expansion period of the ellipse *always* toward rotator orbits. As a consequence, particles that turn from librator into rotator orbits accumulate collisions that effectively reduce their velocity and scatter them beyond the separatrix, thereby explaining the low escape velocities of particles with escape times $t_{esc}>10$. One might think of using this mechanism to slow down particles.

B. Distributions of the escape velocities

In Fig. 18, the distribution of the escape velocities is shown for different values of C (IVE). With increasing amplitude, the mean escape velocity $\langle|\boldsymbol{v}(t_{esc})|\rangle$ is shifted toward larger values. Since on average there are slightly more collisions with the contracting ellipse than with the expanding one, a larger driving amplitude leads to an increased mean energy of the particles. The sharp peak at $|\boldsymbol{v}|=1$ corresponds to the particles that leave the billiard without a single collision with the boundary; thus $|\boldsymbol{v}_{esc}|=|\boldsymbol{v}_0|=1$.

In the case of the HVE (see Fig. 19), the distribution looks quite different. The majority of the particles have an escape velocity smaller than $|\boldsymbol{v}_0|=100$, and especially at the lowest accessible escape velocity $|\boldsymbol{v}_{esc}|\approx 97$ there is a large peak. This is due to the fact that the ellipse starts with an expanding motion which deprives the particles of energy upon boundary collisions, and a large fraction of particles decays during that first expansion period. Around $t=\pi/2$, in the vicinity of the first turning point, the ellipse stays comparatively long (boundary velocity ≈ 0), and more particles escape, leading to the large peak at $|\boldsymbol{v}|\approx 97$. The asymmetric shape of the distribution is additionally reinforced since the librators that escape also have low energies. The particles that have not escaped after 2.5×10^4 accumulated collisions during the expanding and contracting motion of the ellipse and the fluctuations in the energy transfer lead to a roughly uniform distribution. The distributions for higher values of C look very much like the one shown in the case $C=0.05$, except that they get wider with increasing amplitude.

Since most of the particles leaving the ellipse have velocities smaller than $|\boldsymbol{v}_0|$, the question arises whether the billiard could be used for systematic velocity lowering. To enforce this effect, one could try, e.g., to choose asymmetric driving laws. We point out that the lowered energy of the escaping particles is a feature of the dynamics of the ellipse. In general (concerning other geometries), particles are more likely to strike a contracting than a receding boundary, which leads one to expect increased energies of the escaping particles.

VI. CONCLUDING REMARKS

We investigated the classical dynamics of the static and especially the driven elliptical billiard with an emphasis on the escape rate of an ensemble of particles. As predicted in Ref. [5] in a general context for integrable billiards, we found an algebraic decay in the long-time behavior of the static ellipse, due to the integrable structure of the underlying dynamics. Besides the energy, the product of the angular momenta $F(\varphi,p)$ about the two foci is preserved. The sign of the initial value of F determines whether a particle moves on a rotator or librator orbit and only the rotators are always (for all hole positions) connected with the hole. Consequently, the decay approaches a saturation value $N_s(\varepsilon)$, which is maximal for the hole lying at the short side of the ellipse; at this hole position none of the librators are connected with it. $N_s(\varepsilon)$ depends on the numerical eccentricity ε of the ellipse, and we predicted this dependence very accurately from theoretical considerations. As a consequence, varying ε allows us to control the number of emitted particles.

When applying harmonic boundary oscillations, neither the energy nor $F(\varphi,p)$ will remain a constant of the motion. We performed numerical simulations for two different ensembles, representing the two important borderline cases: first, the intermediate-velocity ensemble, where $|\boldsymbol{v}_0|\approx\omega A$ (ωA being the boundary velocity), and second the high-

velocity ensemble, where $|\boldsymbol{v}_0| \gg \omega A$. In both cases we observed an initial fast decay with an ensuing transition period, followed by a nonvanishing (even for large times) near-algebraic decay. The emission rate depends monotonically on the driving amplitude. The changes of $F(\varphi,p)$ of particles upon a single collision with the boundary are much smaller in the case of the HVE, due to the high velocities of the particles. As a consequence, the resulting decay is similar to that of the static system. The observed disappearance of the saturation value in both ensembles is due to the gradual destruction of the librator orbits caused by two fundamental processes: The vertical processes, where upon collision momentum normal to the boundary is transferred, making changes in the sign of $F(\varphi,p)$ possible; and the horizontal processes where the particle hits the ellipse due to the boundary motion at a different position (compared to the static case), leading again to changes in $F(\varphi,p)$ that can result in the transition of a librator into a rotator. Just as in the static system, particles starting on rotator orbits $[F(\varphi_0,p_0)<0]$ cause the initial fast decay. With increasing time, more and more particles with initial conditions closer and closer to the elliptic fixed points can escape, due to the vertical and horizontal processes just described, and cause the nonvanishing emission rate in the long-time behavior of the decay. We confirmed this strong connection between the escape time and $F(\varphi_0,p_0)$ by analyzing this quantity carefully. In the HVE, the escape rate as well as correlations of the escape time and the PAM are modulated with the same period as the breathing of the ellipse; the ellipse acts as a pulsed source.

Concerning escape velocities, an astonishing feature is observed in the case of the HVE: the distribution of the escape velocities is highly asymmetric and particles escape mainly with $|\boldsymbol{v}(t_{esc})|<|\boldsymbol{v}_0|$; the driven ellipse could be used for systematic cooling. To avoid escape velocities bigger than $|\boldsymbol{v}_0|$, the use of a point source as an initial ensemble seems reasonable. Simulations with thermal ensembles suggested the ellipse as a state transformer; thermal ensembles were changed into nonthermal ones. Furthermore, the ellipse could be used as a controllable source of particles: if a certain emission rate is required, this can be achieved by tuning the driving amplitude, whereas the numerical eccentricity ε of the static ellipse allows us to emit a certain number of particles.

ACKNOWLEDGMENTS

Valuable discussions with A. Richter, V. Constantoudis, A. Karlis, and M. Oberthaler are gratefully acknowledged. F.L. acknowledges support from the Landesgraduiertenförderung Baden-Württemberg. F.K.D. wishes to thank the DAAD for financial support in the framework of a visit to the University of Heidelberg.

[1] M. V. Berry, Eur. J. Phys. **2**, 91 (1982).
[2] H.-J. Stöckmann, *Quantum Chaos: An Introduction* (Cambridge University Press, Cambridge, U.K., 1999).
[3] M. C. Gutzwiller, *Chaos in Classical and Quantum Mechanics* (Springer, New York, 1990).
[4] D. A. Egolf, Science **287**, 101 (2000).
[5] W. Bauer and G. F. Bertsch, Phys. Rev. Lett. **65**, 2213 (1990).
[6] L. A. Bunimovich, Commun. Math. Phys. **65**, 295 (1979).
[7] V. Milner, J. L. Hanssen, W. C. Campbell, and M. G. Raizen, Phys. Rev. Lett. **86**, 1514 (2001).
[8] H. D. Gräf, H. L. Harney, H. Lengeler, C. H. Lewenkopf, C. Rangacharyulu, A. Richter, P. Schardt, and H. A. Weidenmüller, Phys. Rev. Lett. **69**, 1296 (1992).
[9] J. Stein and H.-J. Stöckmann, Phys. Rev. Lett. **68**, 2867 (1992).
[10] C. M. Marcus, A. J. Rimberg, R. M. Westervelt, P. F. Hopkins, and A. C. Gossard, Phys. Rev. Lett. **69**, 506 (1992).
[11] J. U. Nöckel and A. D. Stone, Nature (London) **385**, 45 (1997).
[12] G. M. Zaslavsky, Phys. Today **52** (8), 39 (1999).
[13] L. A. Bunimovich and C. P. Dettmann, Phys. Rev. Lett. **94**, 100201 (2005).
[14] A. Pais, *Niels Bohr's Times—Physics, Philosophy and Policy* (Oxford University Press, Oxford, 1991).
[15] G. Abal, R. Donangelo, and C. O. Dorso, Phys. Rev. C **46**, 380 (1992).
[16] J. Koiller, R. Markarian, S. O. Kamphorst, and S. P. de Carvalho, J. Stat. Phys. **83**, 127 (1996).
[17] N. Friedman, L. Khaykovich, R. Ozeri, and N. Davidson, Phys. Rev. A **61**, 031403(R) (2000).
[18] A. Kaplan, N. Friedman, M. Andersen, and N. Davidson, Phys. Rev. Lett. **87**, 274101 (2001).
[19] N. Friedman, A. Kaplan, D. Carasso, and N. Davidson, Phys. Rev. Lett. **86**, 1518 (2001).
[20] M. F. Andersen, A. Kaplan, N. Friedmann, and N. Davidson, J. Phys. B **35**, 2183 (2002).
[21] A. J. Lichtenberg and M. A. Liebermann, *Regular and Chaotic Dynamics* (Springer-Verlag, New York, 1992).
[22] A. Y. Loskutov, A. B. Ryabov, and L. G. Akinshin, J. Exp. Theor. Phys. **89**, 966 (1999).
[23] A. Loskutov, A. B. Ryabov, and L. G. Akinshin, J. Phys. A **33**, 7973 (2000).
[24] A. Loskutov and A. Ryabov, J. Stat. Phys. **108**, 995 (2002).
[25] J. Koiller, R. Markarian, S. O. Kamphorst, and S. P. de Carvalho, Nonlinearity **8**, 983 (1995).
[26] A. P. Itin and A. I. Neishtadt, Regular Chaotic Dyn. **59**, 8 (2003).
[27] A. K. Karlis, P. K. Papachristou, F. K. Diakonos, V. Constantoudis, and P. Schmelcher, Phys. Rev. Lett. **97**, 194102 (2006).
[28] D. Cohen and D. A. Wisniacki, Phys. Rev. E **67**, 026206 (2003).
[29] R. Douady, These de 3eme cycle, Universite Paris VII, 1982 (unpublished).
[30] F. Lenz, F. K. Diakonos, and P. Schmelcher, Europhys. Lett. **79**, 20002 (2007).
[31] S.-J. Chang and R. Friedberg, J. Math. Phys. **29**, 1537 (1988).
[32] H. Alt, H.-D. Gräf, H. L. Harney, R. Hofferbert, H. Rehfeld, A.

Richter, and P. Schardt, Phys. Rev. E **53**, 2217 (1996).
[33] J. D. Meiss and E. Ott, Physica D **20**, 387 (1986).
[34] P. K. Papachristou, F. K. Diakonos, V. Constantoudis, P. Schmelcher, and L. Benet, Phys. Lett. A **306**, 256215 (2002).
[35] P. K. Papachristou, F. K. Diakonos, V. Constantoudis, P. Schmelcher, and L. Benet, Phys. Rev. E **70**, 056215 (2004).
[36] P. L. Kapitsa, Zh. Eksp. Teor. Fiz. **21** (5), 588 (1951).
[37] Since the initial conditions chosen in Sec. III B do not lie on the boundary of the ellipse, the first collision point with the boundary is taken; at this point $t \neq 0$.